# Tailoring of interference-induced surface superconductivity by an applied electric field

Yunfei Bai,[1] Libo Zhang,[2] Xiaobing Luo,[1] A. A. Shanenko,[3] and Yajiang Chen ⬤[1,*]

[1]*Key Laboratory of Optical Field Manipulation of Zhejiang Province, Department of Physics, Zhejiang Sci-Tech University, 310018 Zhejiang, China*

[2]*College of Physics and Optoelectronic Engineering, Hangzhou Institute for Advanced Study, University of Chinese Academy of Sciences, 310024 Zhejiang, China*

[3]*HSE University, 101000 Moscow, Russia*

Nucleation of the pair condensate near surfaces above the upper critical magnetic field and the pair-condensate enhancement/suppression induced by changes in the electron-phonon interaction at interfaces are the most known examples of the surface superconductivity. Recently, another example has been reported when the surface enhancement of the critical superconducting temperature occurs due to quantum interference. In this case the pair states spread over the entire volume of the system while exhibiting the constructive interference near the surface. In the present work we investigate how an applied electric field impacts the interference-induced surface superconductivity. The study is based on a numerical solution of the self-consistent Bogoliubov-de Gennes equations for a one-dimensional attractive Hubbard model. Our results demonstrate that the surface superconducting characteristics, especially the surface critical temperature, are sensitive to the applied electric field and can be tailored by changing its magnitude.

## I. INTRODUCTION

The phenomenon of the surface superconductivity dates back to the classical papers by Saint-James, de Gennes, and Ginzburg [1,2]. Using the Ginzburg-Landau formalism, Saint-James and de Gennes predicted that the nucleation of superconductivity occurs near the surface of the ideal sample in decreasing parallel magnetic fields above the upper critical field. This prediction was confirmed for various superconducting metallic alloys [3–7]. In turn, Ginzburg argued [2] that the surface superconductivity can be significantly different from the bulk one when the phonon properties at surfaces/interfaces are altered as compared to the bulk lattice vibrations. Relevant examples and confirmations range from thin films to small superconductive particles [8–11].

Much less is known about the surface superconductivity in the absence of magnetic fields and surface phonon modes. The surface superconducting pair potential (gap function) can indeed be larger (up to $\sim 20\%$) than its bulk value [12–16]. However, the relative difference $[\tau = (T_{cs} - T_{cb})/T_{cb}]$ between the surface superconducting critical temperature $T_{cs}$ and the bulk one $T_{cb}$ was found to be negligible in those cases. In more details, it was established [13] that $\tau$ is exactly zero for the standard BCS interaction of electrons (attraction in the Debye window near the Fermi surface) while it can go up to $\sim 10^{-3}$ when combining the attraction in the Debye window with the repulsion at high energies.

Recently, it has been demonstrated that $\tau$ can increase up to about 25% within the attractive Hubbard model at the half filling [17–19]. The comprehensive study [20] of all the contributions to the gap function has demonstrated that the origin of this effect is the constructive interference of the pair modes near the sample surface. It was revealed that all the self-consistent pair states contributing to the gap function are delocalized and occupy the entire volume of the system [20,21]. The condensation of Cooper pairs near the sample surface above the bulk critical temperature occurs due to the quantum interference of the pair states: it is destructive in bulk and constructive near surfaces. Exactly the superposition of all the contributing pair states is responsible for the effect of interest. Moreover, the impact of the interference-induced surface superconductivity can be further enhanced by tuning the Debye frequency [22] due to the removal of the contribution of high-energy quasiparticles. As a result, $\tau$ can be enlarged up to $60\% \sim 70\%$. However, this value can be reduced for more sophisticated variants of the surface confining potential (as compared to the standard infinite single-electron potential barrier) [23].

Experimentally and theoretically, it is of great importance to investigate the response of the interference-induced surface superconducting state to other controllable parameters, in particular, to an electric field. The latter is one of the most useful tools of modifying properties of thin superconductors and surface pair states in bulk samples [24–27]. For example, an electric-field-induced shift of $T_c$ was observed in Sn, In, and NbSe$_2$ thin films [24,28,29]. Moreover, the electric field can also give rise to the multigap structure of the surface pair states [30] and result in the superconductor-metal [31,32] and superconductor-insulator transitions [33–35].

In the present work, we investigate the effect of an external electric field on the interference-induced surface

*yjchen@zstu.edu.cn

superconductivity within a one-dimensional attractive Hubbard model at the half-filling level. By numerically solving the self-consistent BdG equations, we demonstrate that varying the field strength makes it possible to fine tune the surface superconducting properties, changing the surface critical temperature in a wide range of its values. Here we note that the interference-induced surface superconductivity is not sensitive to the system dimensionality [22] and appears in 2D and 3D systems [18], where the superconductive fluctuations are much less important as compared to the 1D case. Thus, to simplify our study, we investigate the 1D chain, expecting that our mean-field results are relevant for higher dimensions.

The paper is organized as follows. In Sec. II we outline the BdG formalism for a one-dimensional attractive Hubbard model in the presence of a screened electric field parallel to the chain of atoms. Our numerical results and related discussions are presented in Sec. III. Concluding remarks are given in Sec. IV.

## II. THEORETICAL FORMALISM

Similarly to the previous papers on the interference-induced surface superconductivity [20,22,23], we investigate an attractive Hubbard model for a one-dimensional chain of atoms with the grand-canonical Hamiltonian given by [19,36,37]

$$H - \mu N_e = -\sum_{i\delta\sigma} t_\delta c^\dagger_{i+\delta,\sigma} c_{i\sigma} + \sum_{i\sigma}[U(i) - \mu]n_{i\sigma}$$
$$- g\sum_i n_{i\uparrow}n_{i\downarrow}, \tag{1}$$

where $i$ is the site index, $c_i$ and $c^\dagger_i$ are the electron annihilation and creation operators associated with site $i$, $N_e$ and $n_{i\sigma}$ are the total and local electron number operators, $g$ denotes the on-site attractive interaction ($g > 0$), $U(i)$ and $\mu$ are the one-electron and chemical potentials, respectively, and $t_\delta$ is the hopping amplitude between sites $i$ and $i + \delta$. We adopt the nearest neighbor hopping, i.e., $\delta = \pm 1$ and $t_\delta = t$. The open boundary conditions are applied in the present study so that the relevant wave functions vanish at $i = 0$ and $N + 1$.

The single-electron potential $U(i)$ is the potential energy of an electron in the external electric field $\mathbf{E}(i)$ that is parallel to the chain and along its positive direction. The field magnitude is given by

$$E(i) = E_0[e^{-i/\lambda} + e^{-(N+1-i)/\lambda}]$$
$$= 2E_0 e^{-(N+1)/2\lambda} \cosh[(2i - N - 1)/2\lambda], \tag{2}$$

where $E_0$ is the strength of the screened electric field, and $\lambda$ is the screening length in units of the lattice constant $a$. From Eq. (2) we find

$$U(i) = -2q\lambda E_0 e^{-(N+1)/2\lambda} \sinh[(2i - N - 1)/2\lambda], \tag{3}$$

where $q = -e$, with $e$ the electron charge, and the electric potential is set to nearly zero deep in the chain. The determination of $\lambda$ near the system surface is rather complex. However, as we are interested in the qualitative picture, we can assume, for simplicity, that $\lambda$ is proportional to the Fermi wavelength $\lambda_F$ of the system in the absence of the electric field and electron attractive interactions $g$, i.e., $\lambda \approx \gamma\lambda_F$, with

$\gamma \sim 1$ the parameter of our calculations. Using the dispersion relation [36] $\xi_k = -2t\cos(ka)$, with $ka = n\pi/(N + 1)$, one concludes that the half-filling case corresponds to $\mu = 0$. Then, adopting the parabolic band approximation, one gets $\lambda_F = \sqrt{2}\pi a$. Below our results are shown for $\gamma = 2$ and 5. We remark that our qualitative results are not sensitive to the particular choice of $\gamma$.

The BdG equations ($s$-wave pairing) obtained in the mean-field approximation for the Hamiltonian (1) can be written as [21,22],

$$\epsilon_n u_n(i) = \sum_j h_{ij} u_n(j) + \Delta(i) v_n(i),$$
$$\epsilon_n v_n(i) = -\sum_j h^*_{ij} v_n(j) + \Delta^*(i) u_n(i), \tag{4}$$

where $h_{ij} = -t(\delta_{i,j+1} + \delta_{i,j-1}) + [U(i) - \mu]\delta_{ij}$, $\Delta(i)$ is the superconducting pair potential, $\{\epsilon_n, u_n(i), v_n(i)\}$ are the energy and wave functions of quasiparticles with $n$ the quasiparticle quantum number (here the energy ordering number). The wave functions should be normalized, i.e., $\sum_i |u_n(i)|^2 + |v_n(i)|^2 = 1$, and satisfy the open boundary condition $u_n(0) = u_n(N + 1) = 0$ and $v_n(0) = v_n(N + 1) = 0$. The BdG Eq. (4) are numerically solved together with the self-consistency relation

$$\Delta(i) = g\sum_n u_n(i)v^*_n(i)(1 - 2f_n), \tag{5}$$

where $f_n = f(\epsilon_n)$ is the Fermi-Dirac quasiparticle distribution. The summation above includes positive-energy quasiparticle states inside the Debye window $0 \leqslant \epsilon_n \leqslant \hbar\omega_D$, with $\omega_D$ the Debye frequency. Due to the time reversal symmetry, we regard $\Delta(i)$ as real.

For the half-filling, the chemical potential $\mu$ is fixed by the relation

$$\bar{n}_e = 1 = \frac{1}{N}\sum_i n_e(i), \tag{6}$$

where the electron occupation number $n_e(i)$ is given by

$$n_e(i) = \frac{2}{N}\sum_n [f_n|u_n(i)|^2 + (1 - f_n)|v_n(i)|^2]. \tag{7}$$

In our calculations we use the microscopic parameters $g = 2$, $\hbar\omega_D = 10$, and $N = 301$. For this choice, $\tau = (T_{cs} - T_{cb})/T_{cb} \approx 25\%$ (for zero field). However, as is mentioned above, $\tau$ can be higher for smaller values of the Debye frequency [22]. Notice that $N = 301$ is large enough to avoid any finite size effects. Generally, our qualitative conclusions are not influenced by this choice of the microscopic parameters. Below the energy-related quantities, the electric field and the temperature $T$ are shown in units of $t$, $t/(ea)$, and $t/k_B$, respectively. In our calculations, the self-consistent solution for $\Delta(i)$ is obtained with the accuracy of $10^{-8}$.

### III. RESULTS AND DISCUSSIONS

#### A. Suppression of $T_{cs}$ by electric fields

In Fig. 1(a) one can find a typical example of the self-consistent pair potential $\Delta(i)$ given as a function of the site number $i$. It is calculated for the electric-field strength
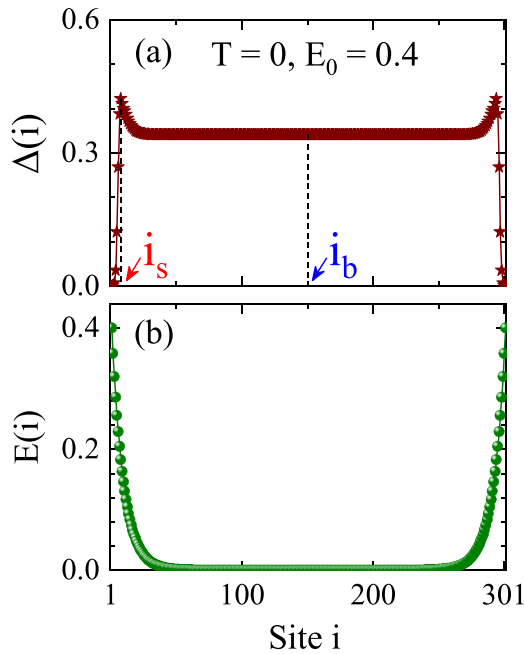
FIG. 1. (a) The spatial profile of $\Delta(i)$ at $T = 0$, $E_0 = 0.4$, and $\gamma = 2$. The site $i_s$ corresponds to the surface maximum of the pair potential, and $i_b = (N + 1)/2$ marks the center of the chain. (b) The screened electric field versus $i$ for $E_0 = 0.4$ and $\gamma = 2$.

$E_0 = 0.4$ at $T = 0$. The spatial profile of $\Delta(i)$ demonstrates that the pair potential (the gap function or the order parameter) stays nearly uniform inside the chain. It is close to $\Delta(i_b) = 0.340$, where $i_b = (N + 1)/2$. Below, $\Delta(i_b)$ is regarded as the bulk pair potential. However, near the surface, the gap function exhibits a maximum. Its value $\Delta_{\max} = 0.422$ is 24.1% higher than $\Delta(i_b)$. The locus of the maximum is labeled as $i_s$, and here $i_s = 9$. The profile of the screened electric field is shown for $E_0 = 0.4$ in Fig. 1(b). The field vanishes in the region $i \in [50, 250]$. Obviously, the maximum of the pair potential is located in the domain of the exponential decay of the field.

Figures 2(a)–2(d) show $\Delta(i_s)$ and $\Delta(i_b)$ as functions of $T$ for $E_0 = 0, 0.1, 0.2$, and $0.4$, respectively. The temperature profiles of $\Delta(i_s)$ and $\Delta(i_b)$ are similar to the general temperature dependence of the BCS gap, however, each of these quantities drops to zero at a distinct critical temperature dependent on $E_0$. As a result, one obtains the surface $T_{cs}$ and bulk $T_{cb}$ critical temperatures [19,20]. At $E_0 = 0$, we find $T_{cb} = 0.199$ and $T_{cs} = 0.246$ in agreement with the results reported in Ref. [22]. One notes that $T_{cb}$ does not depend on the field strength. Physically, this is clear as the screened electric field vanishes in the center of the chain at $i = i_b$. Therefore, $\Delta(i_b)$ does not change under the influence of the screened electric field together with the bulk critical temperature $T_{cb}$. In contrast, $T_{cs}$ is significantly affected by the field. Indeed, $T_{cs}$ decreases by about 14% (from 0.246 to 0.212) as $E_0$ increases from 0 to 0.4.

To go into more detail on the dependence of our results on $E_0$, $T_{cs}$, $T_{cb}$, and the relative enhancement of the surface superconducting temperature $\tau = (T_{cs} - T_{cb})/T_{cb}$ are shown versus $E_0$ in Fig. 3. For comparison, the data are given for the two
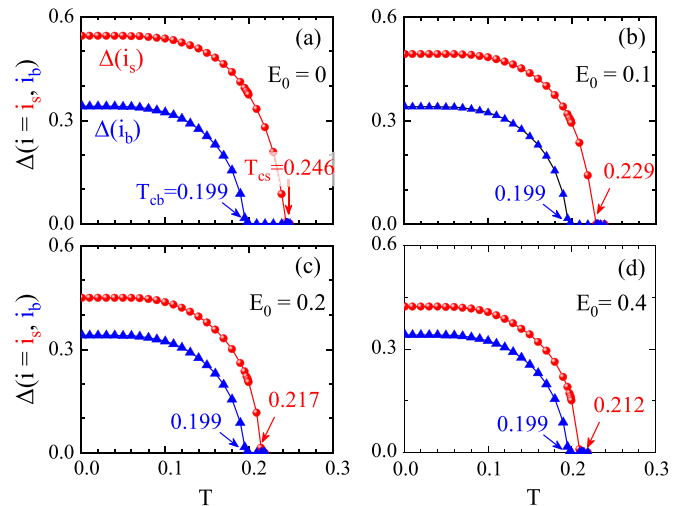


FIG. 2. The surface and bulk pair potentials $\Delta(i = i_s, i_b)$ versus the temperature $T$ at $E_0 = 0$ (a), 0.1 (b), 0.2 (c), and 0.4 (d) for $\gamma = 2$. The surface and bulk critical temperatures $T_{cs}$ and $T_{cb}$ are defined as the temperatures at which $\Delta(i_s)$ and $\Delta(i_b)$ approach zero.

$\gamma$ values: $\gamma = 2$ and 5. For $\gamma = 2$, one can see from Fig. 3(a) that $T_{cs}$ decreases monotonically from 0.246 at $E_0 = 0$ to 0.212, and at $E_0 = E_0^* = 0.3$. A further increase of $E_0$ does not have any effect on $T_{cs}$ and it remains equal to 0.212 for $E_0^* \leqslant E \leqslant 1$. The corresponding relative enhancement of $T_{cs}$ [see Fig. 3(b)] decreases from 23.8% at $E_0 = 0$ to 6.6% at $E_0 = E_0^*$ and then stays the same for $E_0 > E_0^*$. Thus, we find that the interference-induced surface superconductivity and its critical temperature can be fine-tuned by changing the applied electric field. For the chosen microscopic parameters this fine tuning is within the range $\approx 7-24\%$. However, for smaller
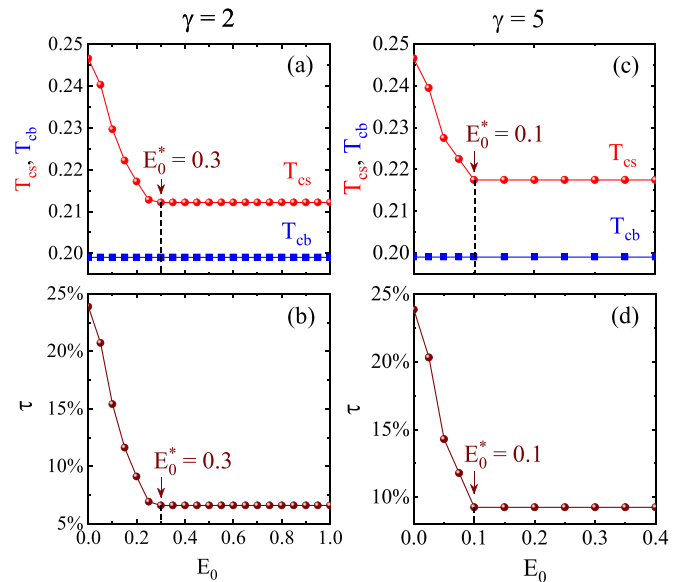


FIG. 3. (a), (c) The surface $T_{cs}$ and bulk $T_{cb}$ critical temperatures versus the field strength $E_0$ for the screening length ratio $\gamma = 2$ and 5. (b), (d) The corresponding relative enhancement of the surface critical temperature $\tau = (T_{cs} - T_{cb})/T_{cb}$ as a function of $E_0$. $E_0^*$ denotes the field strength above which $T_{cs}$ and $\tau$ do not change with $E_0$.
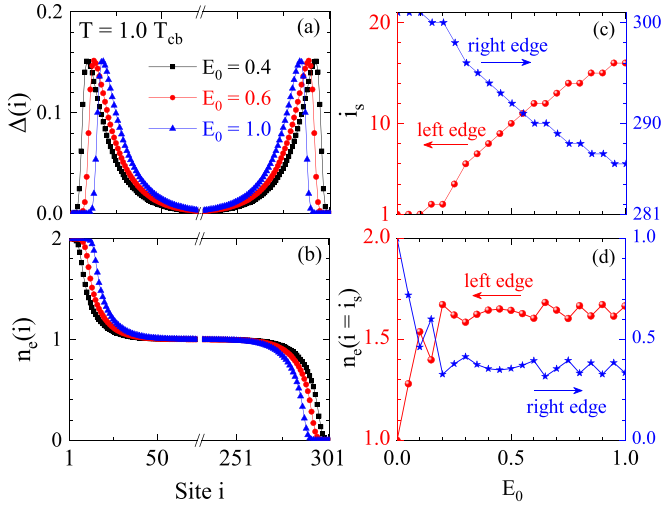
FIG. 4. (a), (b) $\Delta(i)$ and $n_e(i)$ as functions of $i$, calculated at $T = 1.0\,T_{cb}$; $\gamma = 2$ for $E_0 = 0.4$ (black squares), 0.6 (red circles), and 1.0 (blue triangles). (c) The locus $i_s$ of the pair-potential maximum near the right (blue stars) and left edges (red spheres) versus $E_0$, as calculated for $T = 1.0\,T_{cb}$, $\gamma = 2$. (d) The corresponding electron occupation number at $i = i_s$ near the right and left edges versus $E_0$; the colors and symbols are the same as in panel (c).



FIG. 5. The local pair potentials $\Delta(i = 1, 301)$ (a) and electron occupation number $n_e(i = 1, 301)$ (b) as functions of $E_0$ at $T = 0$ for $\gamma = 2$. Panels (c) and (d) are the data for $\gamma = 5$. The red stars correspond to $i = 1$ while the blue spheres are for $i = 301$. The definition of $E_0^*$ is the same as that in Fig. 3.

Debye frequencies the upper level of this range can increase up to 60–70% at zero electric field, see Ref. [22].

For $\gamma = 5$, as seen from Figs. 3(c) and 3(d), we also find that $T_{cs}$ and $\tau$ decrease with increasing $E_0$ for $E_0 < E_0^*$. However, such a decrease is now terminated at significantly weaker fields. In particular, we find that $E_0^* = 0.1$. This is because larger values of $\gamma$ correspond to larger penetrations of the electric field (less screening). As a result, the reconstruction of the surface pair states is completed at smaller fields, and the saturation values of $T_{cs}$ ($= 0.218$) and $\tau$ ($= 9.3\%$) are larger than those obtained for $\gamma = 2$, compare Figs. 3(a) and 3(b), and Figs. 3(c) and 3(d).

It is important to emphasize that the position of the pair-potential maximum, i.e., $i_s$, changes with $E_0$. This is clearly seen from Fig. 4(a), where the spatial profile of $\Delta(i)$ is shown for $T = T_{cb}$, $\gamma = 2$, and $E_0 = 0.4$, 0.6, and 1.0. One can see that the surface enhancement of the pair potential is most pronounced at $i = i_s$, and its maximum shifts toward the chain center with increasing $E_0$. More precisely, there are two surface maxima: one is close to the left edge and another is located near the right edge. Both of them shift toward the chain center with increasing $E_0$. So, there are two values of $i_s$, one of them (near the left edge) increases with $E_0$ while another (near the right edge) decreases, as shown in Fig. 4(c).

In fact, the electric-field surface effect is even more complicated than one might expect from Figs. 4(a) and 4(c). From Figs. 4(b) and 4(d), one can see that the electron spatial distribution $n_e(i)$ is significantly altered in the presence of the field. While $n_e(i)$ remains equal to one (the half-filling regime) in the center of the chain, electrons are removed from its right edge and accumulate at the left one, see Fig. 4(b). In particular, the sites near the right edge become completely empty while those near the left edge are fully occupied by electrons [$n_e(i) = 2$]. This indicates the emergence
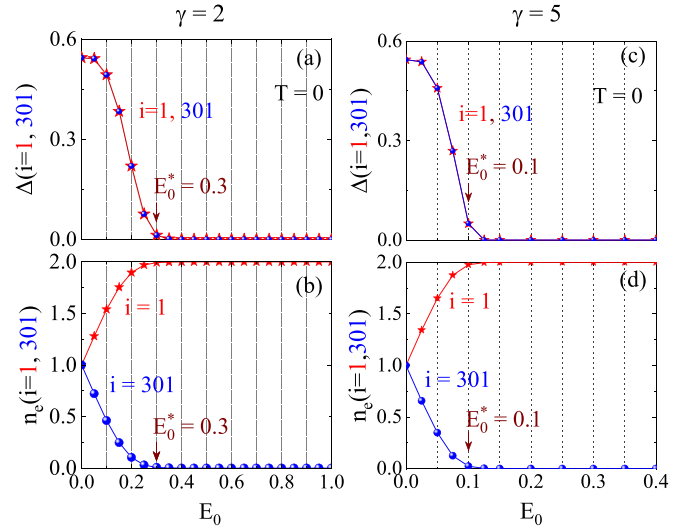
of the superconductor-insulator surface transition, which agrees with the findings of Ref. [38]. Thus, we obtain two domains near the system edges: the first one (closer to the edges) is in the insulating regime while the second domain exhibits an enhanced superconducting temperature in comparison with the bulk critical temperature.

Additional insight is provided by Fig. 5, where the pair potential and electron occupation number at the first ($i = 1$) and last ($i = 301$) sites of the chain are shown versus $E_0$ at $T = 0$ for $\gamma = 2$ and 5. One can learn from Fig. 5 that the field strength $E_0 = E_0^*$, above which $T_{cs}$ remains the same, is connected with the onset of the surface insulator state [38]. In particular, the pair potentials at sites $i = 1$ and 301 are close to zero at $E_0 = E_0^* = 0.3$ for $\gamma = 2$ and $E_0 = E_0^* = 0.1$ for $\gamma = 5$, see Figs. 5(a) and 5(c). In turn, at the same time $n_e(i = 1)$ and $n_e(i = 301)$ approach two (fully occupied) and zero (completely empty), respectively, see Figs. 5(b) and 5(d).

One can also learn from Figs. 4(b) and 4(d) that for $E_0 > E_0^*$, the electron spatial distribution remains nearly the same in the vicinity of $i_s$. For example, this is clearly seen in Fig. 4(d), where $n(i_s)$ is given versus $E_0$ for the vicinity of the left and right chain edges. As a result, $\Delta(i_s)$, which is directly connected with $T_{cs}$, does not change with $E_0$ for $E_0 > E_0^*$, and this explains why $T_{cs}$ stays the same above $E_0^*$.

### B. Microscopic mechanism behind the suppression of surface superconductivity

Now we investigate the microscopic mechanism underlying the suppression of the surface superconductivity induced by a screened electric field, based on the analysis of the quasiparticle contributions to the pair potential at $T = 0$. To facilitate our study, we introduce the cumulative pair potential defined as [20]

$$\Delta^{(\epsilon)}(i) = g \sum_{0 \leqslant \epsilon_n \leqslant \epsilon} u_n(i) v_n^*(i)(1 - 2f_n). \quad (8)$$
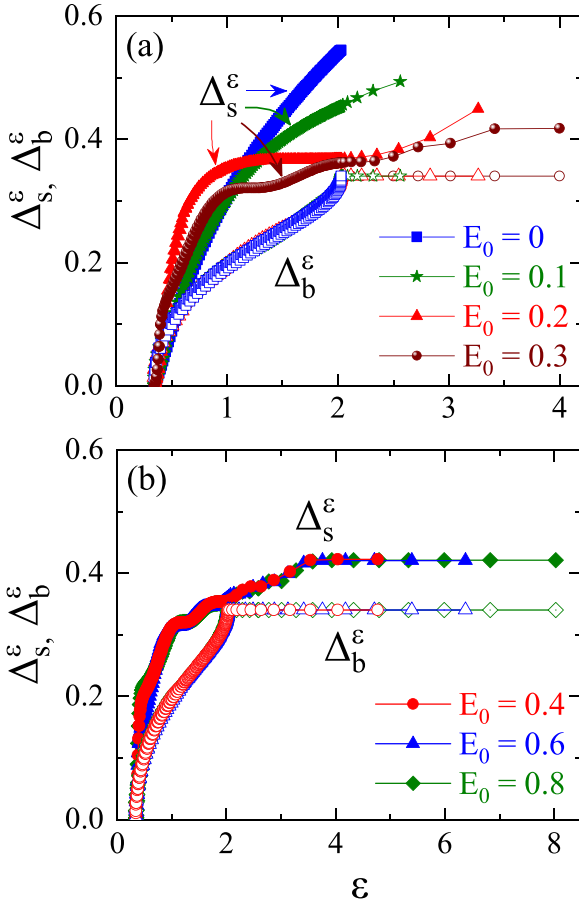
FIG. 6. The cumulative pair potentials $\Delta_s^\epsilon \equiv \Delta^{(\epsilon)}(i_s)$ and $\Delta_b^\epsilon \equiv \Delta^{(\epsilon)}(i_b)$ versus the quasiparticle energy $\epsilon$ at $T = 0$ and $\gamma = 2$: panel (a) demonstrates the results for $E_0 = 0, 0.1, 0.2, 0.3$; panel (b) shows the data for $E_0 = 0.4, 0.6, 0.8$. The solid symbols correspond to $\Delta_s^\epsilon$ while the open ones are for $\Delta_b^\epsilon$.

Below we consider the cumulative pair potential at $i = i_s$ and $i_b$. To simplify the notations, $\Delta^{(\epsilon)}(i = i_s)$ and $\Delta^{(\epsilon)}(i = i_b)$ are referred to as $\Delta_s^\epsilon$ and $\Delta_b^\epsilon$, respectively.

Figure 6 demonstrates $\Delta_s^\epsilon$ and $\Delta_b^\epsilon$ as functions of the upper limit of the quasiparticle energy $\epsilon$ for the field strengths $E_0 = 0, 0.1, 0.2, 0.3, 0.4, 0.6,$ and $0.8$ at $T = 0$. The results for $\Delta_s^\epsilon$ are shown by the solid symbols while those for $\Delta_b^\epsilon$ are given by the open symbols. As seen from Fig. 6, all the quasiparticles have energies less than $\hbar\omega_D$ and so every positive-energy quasiparticle state gives a contribution to the pair potential, according to Eq. (5). For $E_0 = 0$ [see the blue open squares in Fig. 6(a)], one finds that the dependence of $\Delta_b^\epsilon$ on $\epsilon$ reflects the energy dependence of the quasiparticle density of states (DOS) $D(\epsilon) = d\nu/d\epsilon$, with $d\nu$ the number of quasiparticles in the energy interval $d\epsilon$. $D(\epsilon)$ is proportional to the single-electron DOS $N(\xi) = d\nu/d\xi$, with $\xi$ the single-particle energy measured from the chemical potential $\mu$ ($\mu = 0$ for the half-filling case at zero field). Employing the simple BCS approximation $\epsilon = \sqrt{\xi^2 + \Delta_0^2}$, with $\Delta_0$ the excitation gap (the minimal quasiparticle energy), one finds $D(\epsilon) = N(\xi)\epsilon/\sqrt{\epsilon^2 - \Delta_0^2}$. Due to the van Hove singularities at the lower and upper electron band edges, one obtains $N(\xi = \pm 2) \to \infty$. In addition, $\epsilon/\sqrt{\epsilon^2 - \Delta_0^2} \to \infty$,

as $\epsilon$ approaches $\Delta_0$. Therefore, $\Delta_b^\epsilon$ has infinite derivatives at $\epsilon = \Delta_0 \approx 0.3\text{-}0.4$ and $\epsilon = 2$.

When switching on the electrostatic field, we observe a similar dependence on $\epsilon$ for $\epsilon \leqslant 2$, as seen from the data for $\Delta_b^\epsilon$ in Figs. 6(a) and 6(b). However, for $E_0 > 0$ there appear high-energy quasiparticles with $\epsilon_n > 2$ that do not produce any contribution to $\Delta_b^\epsilon$. This is seen from the flat profile $\Delta_b^\epsilon = 0.34$ for $\epsilon > 2$. Then, based on Fig. 6(a), we conclude that the bulk pair potential does not change with increasing $E_0$, though there are high-energy quasiparticles induced by the screened electric field. This conclusion is in agreement with our present results for $T_{cb}$ given in Fig. 3(a).

The response of the cumulative pair potential at $i = i_s$ ($\Delta_s^\epsilon$) to the screened electric field is more complex. Here, when $E_0$ increases from 0 to 0.1, $\Delta_s^\epsilon$ remains nearly the same in the low-energy sector $\epsilon < 1.2$. However, its value decreases significantly as compared to that of $E_0 = 0$ for the energies $1.2 < \epsilon < 2$. This decrease is partly compensated by the appearance of the quasiparticle contributions with $\epsilon > 2$. The dependence of $\Delta_s^\epsilon$ on $\epsilon$ demonstrates further evolution at $E_0 = 0.2$. Its overall increase with $\epsilon$ becomes more pronounced for $\epsilon < 1.2$, as compared to the case of $E_0 = 0.1$. Then, $\Delta_s^\epsilon$ stays nearly flat for $1.2 < \epsilon < 2$, with $\Delta_s^\epsilon \approx 0.367$, while it slightly increases with $\epsilon$ for the high-energy regime with $\epsilon > 2$. For $E_0 = 0.3$, the spatial profile of $\Delta_s^\epsilon$ becomes even more complex. One can see the presence of three flat regions around the points $\epsilon = 0.2, 2,$ and $3.5$. Quasiparticles with the corresponding energies do not contribute to the surface superconducting state.

Finally, for $E_0 > 0.3$ the results for $\Delta_s^\epsilon$ does not change any more, which is in agreement with our finding that $T_{cs}$ does not change with $E_0$ for $E_0 > E_0^* = 0.3$, see Fig. 3. One can see from Fig. 6(b) that in this regime $\Delta_s^\epsilon$ exhibits a faster overall increase with $\epsilon$ for low energies, as compared to the corresponding increase of $\Delta_b^\epsilon$. The surface cumulative pair potential reaches the values 0.42 at $\epsilon = 4.0$ and stays the same for $\epsilon > 4.0$. A similar high-energy behavior is obtained for the bulk cumulative pair potential. However, it saturates at the smaller value 0.34 when $\epsilon$ exceeds 2.0. This is in agreement with the fact that for $E_0 > E_0^*$ we find $T_{cs}$ larger than $T_{cb}$ by 6.6%. Thus, our study demonstrates that the alterations of the quasiparticle contributions with $\epsilon > 1.2$ are responsible for the changes of the surface states in the presence of the external electric field.

A further insight is obtained when analyzing the single-species quasiparticle contribution to the pair potential given by

$$\Delta_n(i) = g u_n(i) v_n^*(i)(1 - 2f_n). \tag{9}$$

Figure 7 shows $\Delta_n(i)$, $u_n(i)$, and $v_n(i)$ for four quasiparticle species with $\epsilon_n = 0.6$ [panels (a1)–(a3)], 1.41 [panels (b1)–(b3)], 2.21 [panels (c1)–(c3)], and 3.27 [panels (d1)–(d3)]. The results are obtained for $E_0 = 0.2 < E_0^*$. In this case, the left maximum of $\Delta(i)$ is located at $i_s = 2$. For $\epsilon_n = 0.6$, see Figs. 7(a1)–7(a3), $\Delta_n(i)$ is a strongly oscillating function of $i$, together with $u_n(i)$ and $v_n(i)$. Here we find that $\Delta_n(i_s) = 0.01$ (it reaches its local maximum), whereas $\Delta_n(i_b) = 0.009$. This highlights the fact that the low-energy quasiparticles give almost the same contribution to the surface and bulk superconductivity for sufficiently small fields, i.e., the screened
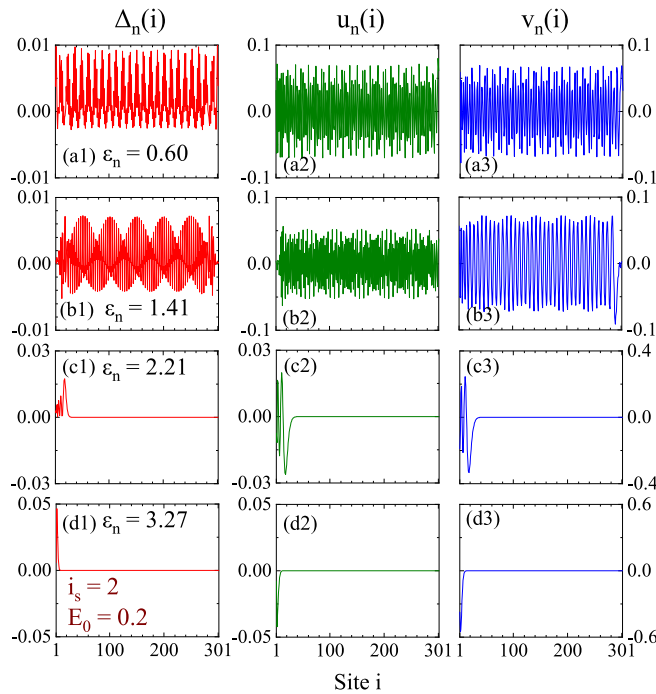
FIG. 7. The single-species quasiparticle contribution $\Delta_n(i)$ and the quasiparticle wave functions $u_n(i)$ and $v_n(i)$ for $\epsilon_n = 0.60$ (a), 1.41 (b), 2.21 (c), and 3.27 (d), as calculated at $E_0 = 0.2$, $T = 0$, and $\gamma = 2$. Panels (a1)–(d1) demonstrate $\Delta_n(i)$; panels (a2)–(d2) and (a3)–(d3) give the corresponding $u_n(i)$ and $v_n(i)$, respectively. In this case, the maximum of $\Delta(i)$ is located at $i_s = 2$.

electric field does not significantly affect the contributions of these quasiparticles to the pair potential. For $\epsilon_n = 1.41$, see Figs. 7(b1)–7(b3), the surface-superconductivity contribution is nearly suppressed. Indeed, we have $\Delta_n(i_s) = 7.6 \times 10^{-5}$, as compared to $\Delta_n(i_b) = 7.1 \times 10^{-3}$. Such a small value of $\Delta_n(i_s)$ corresponds to the first flat regime of $\Delta_s^\epsilon$ around the energy $\epsilon \approx 1.2$ in Fig. 6. At the same time $\Delta_b^\epsilon$ is still significant.

When $\epsilon_n$ exceeds two, the corresponding quasiparticles do not contribute to the bulk superconductivity, i.e., $\Delta_n(i_b)$ becomes negligible, as seen from the examples with $\epsilon_n = 2.21$ and 3.27, shown in Figs. 7(c1)–7(c3) and 7(d1)–7(d3). However, for the surface contribution we have $\Delta_n(i_s) = 1.9 \times 10^{-3}$ (for $\epsilon_n = 2.21$) and $4.6 \times 10^{-2}$ (for $\epsilon_n = 3.27$). The wave functions $u_n(i)$ and $v_n(i)$ for quasiparticles with $\epsilon_n > 2$ are localized near the chain edges due to the presence of the screened electric field, see also Ref. [38].

Figure 8 shows $\Delta_n(i)$, $u_n(i)$, and $v_n(i)$ for the three quasiparticle species with $\epsilon_n = 0.6$ [panels (a1)–(a3)], 2.03 [panels (b1)–(b3)], and 4.77 [panels (c1)–(c3)]. The calculations are performed for $E_0 = 0.4 > E_0^*$. Notice that for this case $i_s = 8$. For $\epsilon_n = 0.6$, the general behavior of $\Delta_n(i)$, $u_n(i)$, and $v_n(i)$ is similar to that of Figs. 7(a1)–7(a3). The results calculated for $\epsilon_n = 2.03$ and demonstrated in Figs. 8(b1)–8(b3) are similar to those in Figs. 7(c1)–7(c3). Finally, the data shown in Figs. 8(c1)–8(c3) do not have a similar dataset in Fig. 7. The point is that Figs. 8(c1)–8(c3) correspond to the quasiparticle species which produces a negligible contribution to the bulk
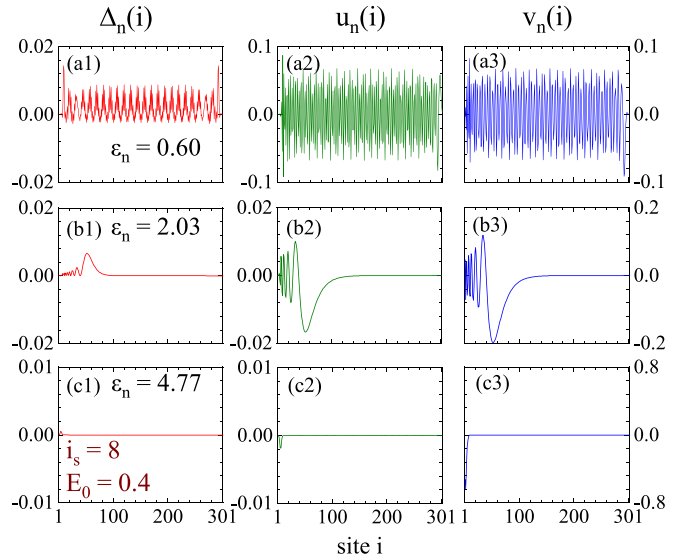


FIG. 8. The same as in Fig. 7 but for $\epsilon_n = 0.60$, 2.03, and 4.77; and $E_0 = 0.4$. Here we have $i_s = 8$.

pair potential [$\Delta_n(i_b) = 4.3 \times 10^{-5}$]. At the same time, its surface contribution is also strongly suppressed. These high-energy quasiparticle species correspond to the long nearly flat regime of $\Delta_s^\epsilon$ illustrated in Fig. 6(b).

## IV. CONCLUSIONS

In summary, we have investigated the effect of an external electrostatic field on the interference-induced surface superconductivity. Our study is based on a self-consistent solution of the Bogoliubov-de Gennes equations for the one-dimensional attractive Hubbard model with the nearest-neighbor hopping at half filling. To reasonably simplify our consideration, a phenomenological expression has been introduced for the screened electric field.

Our results demonstrate that the surface critical temperature $T_{cs}$ is sensitive to the electric field so that the surface superconductivity can be tailored by changing the field strength. It is worth noting that the field shifts the surface maxima of the superconductive pair potential toward the center of the system so that one gets the combination of the surface insulating (closer to the edges) and surface superconducting (further from the edges) domains. When the field strength exceeds its critical value, the surface superconducting temperature does not change any more. In this case, increasing $E_0$ is only accompanied by a further shift of the surface pair-potential maxima toward the chain center. The corresponding maximal value of the pair potential and $T_{cs}$ are not altered.

Finally, our results are discussed for the half filling. However, we note that the qualitative picture remains the same beyond the half filling. In this case, $\tau$ is reduced as compared to its value for the half-filling occupation [20]. As a consequence, we can expect that the critical field strength $E_0^*$ becomes smaller.

## ACKNOWLEDGMENTS

[1] D. Saint-James and P. Gennes, Onset of superconductivity in decreasing fields, Phys. Lett. **7**, 306 (1963).

[2] V. L. Ginzburg, On surface superconductivity, Phys. Lett. **13**, 101 (1964).

[3] G. Bon Mardion, B. Goodman, and A. Lacaze, Lechamp critique de l'etat de surface supraconducteur, Phys. Lett. **8**, 15 (1964).

[4] C. F. Hempstead and Y. B. Kim, Resistive transitions and surface effects in type-II superconductors, Phys. Rev. Lett. **12**, 145 (1964).

[5] W. J. Tomasch and A. S. Joseph, Experimental evidence for a new superconducting phase nucleation field in type-II superconductors, Phys. Rev. Lett. **12**, 148 (1964).

[6] S. Gygax, J. Olsen, and R. Kropschot, Four critical fields in superconducting indium lead alloys, Phys. Lett. **8**, 228 (1964).

[7] M. Strongin, A. Paskin, D. G. Schweitzer, O. F. Kammerer, and P. P. Craig, Surface superconductivity in type I and type II superconductors, Phys. Rev. Lett. **12**, 442 (1964).

[8] M. Strongin, O. F. Kammerer, J. E. Crow, R. D. Parks, D. H. Douglass, and M. A. Jensen, Enhanced superconductivity in layered metallic films, Phys. Rev. Lett. **21**, 1320 (1968).

[9] J. M. Dickey and A. Paskin, Phonon spectrum changes in small particles and their implications for superconductivity, Phys. Rev. Lett. **21**, 1441 (1968).

[10] D. G. Naugle, J. W. Baker, and R. E. Allen, Evidence for a surface-phonon contribution to thin-film superconductivity: Depression of $T_c$ by noble-gas overlayers, Phys. Rev. B **7**, 3028 (1973).

[11] Y. Chen, A. A. Shanenko, and F. M. Peeters, Superconducting transition temperature of Pb nanofilms: Impact of thickness-dependent oscillations of the phonon-mediated electron-electron coupling, Phys. Rev. B **85**, 224517 (2012).

[12] R. J. Troy and A. T. Dorsey, Self-consistent microscopic theory of surface superconductivity, Phys. Rev. B **51**, 11728 (1995).

[13] T. Giamarchi, M. T. Béal-Monod, and O. T. Valls, Onset of surface superconductivity, Phys. Rev. B **41**, 11033 (1990).

[14] A. A. Shanenko and M. D. Croitoru, Shape resonances in the superconducting order parameter of ultrathin nanowires, Phys. Rev. B **73**, 012510 (2006).

[15] L. Lauke, M. S. Scheurer, A. Poenicke, and J. Schmalian, Friedel oscillations and Majorana zero modes in inhomogeneous superconductors, Phys. Rev. B **98**, 134502 (2018).

[16] Y. Chen, Q. Zhu, Q. Liu, and Q. Ren, Nanoscale superconductors: dual Friedel oscillations of single quasiparticles and corresponding influence on determination of the gap energy, Phys. B: Condens. Matter **545**, 458 (2018).

[17] M. Barkman, A. Samoilenka, and E. Babaev, Surface pair-density-wave superconducting and superfluid States, Phys. Rev. Lett. **122**, 165302 (2019).

[18] A. Samoilenka, M. Barkman, A. Benfenati, and E. Babaev, Pair-density-wave superconductivity of faces, edges, and vertices in systems with imbalanced fermions, Phys. Rev. B **101**, 054506 (2020).

[19] A. Samoilenka and E. Babaev, Boundary states with elevated critical temperatures in Bardeen-Cooper-Schrieffer superconductors, Phys. Rev. B **101**, 134512 (2020).

[20] M. D. Croitoru, A. A. Shanenko, Y. Chen, A. Vagov, and J. A. Aguiar, Microscopic description of surface superconductivity, Phys. Rev. B **102**, 054513 (2020).

[21] L. Chen, Y. Chen, W. Zhang, and S. Zhou, Non-gapless excitation and zero-bias fast oscillations in the LDOS of surface superconducting states, Phys. B: Condens. Matter **646**, 414302 (2022).

[22] Y. Bai, Y. Chen, M. D. Croitoru, A. A. Shanenko, X. Luo, and Y. Zhang, Interference-induced surface superconductivity: Enhancement by tuning the Debye energy, Phys. Rev. B **107**, 024510 (2023).

[23] R. H. de Bragança, M. D. Croitoru, A. A. Shanenko, and J. Albino Aguiar, Effect of material-dependent boundaries on the interference induced enhancement of the surface superconductivity temperature, J. Phys. Chem. Lett. **14**, 5657 (2023).

[24] R. E. Glover and M. D. Sherrill, Changes in superconducting critical temperature produced by electrostatic charging, Phys. Rev. Lett. **5**, 248 (1960).

[25] H. Meissner, Search for surface superconductivity induced by an electric field, Phys. Rev. **154**, 422 (1967).

[26] B. Shapiro, Surface superconductivity induced by an external electric field, Phys. Lett. A **105**, 374 (1984).

[27] A. Amoretti, D. K. Brattan, N. Magnoli, L. Martinoia, I. Matthaiakakis, and P. Solinas, Destroying superconductivity in thin films with an electric field, Phys. Rev. Res. **4**, 033211 (2022).

[28] G. Bonfiglioli, R. Malvano, and B. B. Goodman, Search for an effect of surface charging on the superconducting transition temperature of tin films, J. Appl. Phys. **33**, 2564 (1962).

[29] N. E. Staley, J. Wu, P. Eklund, Y. Liu, L. Li, and Z. Xu, Electric field effect on superconductivity in atomically thin flakes of $NbSe_2$, Phys. Rev. B **80**, 184505 (2009).

[30] Y. Mizohata, M. Ichioka, and K. Machida, Multiple-gap structure in electric-field-induced surface superconductivity, Phys. Rev. B **87**, 014505 (2013).

[31] I. Golokolenov, A. Guthrie, S. Kafanov, Y. A. Pashkin, and V. Tsepelin, On the origin of the controversial electrostatic field effect in superconductors, Nat. Commun. **12**, 2747 (2021).

[32] F. Paolucci, F. Crisá, G. de Simoni, L. Bours, C. Puglia, E. Strambini, S. Roddaro, and F. Giazotto, Electrostatic field-driven supercurrent suppression in ionic-gated metallic superconducting nanotransistors, Nano Lett. **21**, 10309 (2021).

[33] K. A. Parendo, K. H. S. B. Tan, A. Bhattacharya, M. Eblen-Zayas, N. E. Staley, and A. M. Goldman, Electrostatic tuning of the superconductor-insulator transition in two dimensions, Phys. Rev. Lett. **94**, 197004 (2005).

[34] K. Ueno, S. Nakamura, H. Shimotani, A. Ohtomo, N. Kimura, T. Nojima, H. Aoki, Y. Iwasa, and M. Kawasaki, Electric-field-induced superconductivity in an insulator, Nat. Mater. **7**, 855 (2008).

[35] R. Yin, L. Ma, Z. Wang, C. Ma, X. Chen, and B. Wang, Reversible superconductor insulator transition in (Li, Fe)OHFeSe flakes visualized by gate-tunable scanning tunneling spectroscopy, ACS Nano **14**, 7513 (2020).

[36] K. Tanaka and F. Marsiglio, Anderson prescription for surfaces and impurities, Phys. Rev. B **62**, 5345 (2000).

[37] K. Takasan and M. Sato, Control of magnetic and topological orders with a DC electric field, Phys. Rev. B **100**, 060408(R) (2019).

[38] L. Yin, Y. Bai, M. Zhang, A. A. Shanenko, and Y. Chen, Surface superconductor-insulator transition induced by an electric field, Phys. Rev. B **108**, 054508 (2023).